Noise effects analysis on subspace-based damage detection with neural networks

Marco Martino Rosso[a], Angelo Aloisio[b], Jonathan Melchiorre[a,*], Fei Huo[a], Giuseppe Carlo Marano[a]

[a] *Politecnico di Torino, DISEG, Department of Structural, Geotechnical and Building Engineering, Corso Duca Degli Abruzzi, 24, Turin, 10128, Italy*
[b] *Civil Environmental and Architectural Engineering Department, Università degli Studi dell'Aquila, via Giovanni Gronchi n.18, L'Aquila, 67100, Italy*

Abstract

Structural health monitoring (SHM) is nowadays a significant and topical issue in the civil engineering field, whose first-level task is the damage detection job. Recent advances in artificial intelligence (AI) combined with non-destructive assessments based on output-only vibration signals represent the frontier of SHM. The present research study has handled an AI-based multi-class damage classification task on a numerical benchmark beam problem with three different procedures. The main purpose was to investigate the noise effects of the analyzed damage detection procedures simulating real-world accelerometer sensors. The first damage identification method leverages simple statistical features of vibration signals, whereas the second method additionally considers a subspace-based damage indicator. The third method relies on a dataset composed of a specific set of damage indicators. Two deep learning (DL) techniques have been adopted to compare and verify the results, i.e. a multi-layer perceptron (MLP) and a one-dimensional convolutional network (1D-CNN). Three groups of different reasonable signal-to-noise ratio (SNR) levels were set up to simulate micro electro-mechanical system (MEMS) accelerometer sensors in real-world conditions to evaluate noise effects. In a nutshell, the results demonstrated that the DL models based on stochastic subspace identification (SSI) methods have good noise immunity performance for damage detection purposes.

Keywords: structural health monitoring, subspace-based damage indicators, signal-to-noise ratio, multi-layer perceptron, convolutional neural network

*Corresponding author.
Email address: jonathan.melchiorre@polito.it (Jonathan Melchiorre)

1. Introduction

Lately, existing infrastructures are experiencing a widespread reduction in safety levels due to the deterioration phenomena of their constitutive materials [70, 23, 69, 37]. During the design process of new infrastructures [41], more specific care is paid to protect materials from degradation, leading to cost-effective designs already accounting for life-cycle assessments [28]. However, structural health monitoring (SHM) procedures still cover an essential role for existing infrastructure heritage [38, 12, 46, 53], both on the direct testing side [1, 25] and non-destructive evaluations (NDE) even denoted as non-destructive testing (NDT) [39, 63, 56, 20, 34]. Innovative cutting-edge approaches rely on emerging advanced sensor technologies, e.g. fiber optic sensors [4, 66], and internet of things edge devices [26, 43]. In the SHM paradigm, the two main worthwhile approaches are acknowledged as model-driven and data-driven [2, 15, 72, 35]. Furthermore, based on the data at disposal, input-output or output-only methods have been developed in recent years to assess the health state of a structure. According to [49], the established techniques within the SHM paradigm may also be categorized into parametric [47, 8], based on analytical time-domain regression models and non-parametric [11], based on statistical data analysis. One of the most widespread output-only approaches for the dynamic behaviour identification of a structural system during operational conditions is acknowledged as operational modal analysis (OMA) [16, 59]. The SHM paradigm has been conceived into five levels [57], corresponding to the knowledge depth of the structure and, i.e., the reliability degree of the health state estimation. Borrowing the terminology from the medical field [7], the first four levels represent a diagnosis phase of the structure under consideration, arranged in damage detection (level 1), damage localization (level 2), damage classification (level 3), and damage severity quantification (level 4). The last fifth level is referred to as the prognosis phase, providing an estimate of the remaining service life. In the present study, the authors analyzed an archetype of SHM level 1 performed with artificial intelligence (AI) and machine learning (ML) techniques, i.e. the neural networks [40, 55]. The proposed damage detection procedure relies on the adoption of damage-sensitive features, i.e. the subspace-based damage indicators, briefly reviewed later in the current manuscript.

However, regardless of the methodology, the quality of SHM outcomes is strongly affected by the characteristics of the sensors employed to collect the vibration response of the structural system of interest. The quality of the estimated modal parameters depends on the quality of information collected from the structural system. In general, the term noise is any undesired signal superimposed on the signal of interest [49]. Different factors and the noise source may affect and corrupt the structural response, e.g. changes in the input excitation (e.g. stochastic nature of traffic load conditions), environmental and climatic agents such as wind, temperature, or even humidity and moisture which may cause sensors damaging and failures, and imperfect intrinsic nature of the sensing system e.g. reading or calibration errors (systematic effects) [50]. Furthermore, in dealing with output-only OMA, operational conditions deliver very low amplitude vibrations and a reliable modal estimation requires low-noise sensors [49].

With the current document, the authors' aim is to numerically simulate a simple beam structure with an array of accelerometer sensors in order to extensively analyze the robustness of the proposed ML-based damage detection in presence of noisy data. To plausibly simulate noise coming from a real sensors array, an additive random noise process usually contaminates the structural time series response collected from each sensor, whose level is quantified by the signal-to-noise ratio (SNR), expressed in decibel (dB) [49]. To better simulate real-world sensors, the authors calibrate different noise levels in order to simulate MEMS accelerometers available on the market, whose characteristics have been retrieved from a market survey and a literature review conducted by the authors of the most widely adopted sensors for SHM purposes. In [58], the authors adopted the subspace-based damage indicators to accomplish the damage localization task with an artificial neural network with the architecture of a multi-layer perceptron (MLP). In that study, the authors do not carry an extensive noise study, since in the first example with 2 degrees of freedom spring-mass system they neglect any noise corruption. In the second example referred to a steel plate, the authors simply considered an additive white Gaussian noise with a SNR of 10dB, without contextualizing their choice. It is worth recalling that the lower the SNR is, the more indistinguishable the signal of interest becomes [49]. In [17], the authors monitored roller bearings in a mechanical system for damage detection tasks accounting for an arbitrarily additive white Gaussian noise with an SNR of 100dB. The authors in [3] provided a study of damage localization with a statistical model-based approach based on a damage detection task with subspace-based indicators. The authors performed a sensitivity analysis of the residual to evaluate modal parameters uncertainties, accounting for Gaussian white noise contaminating response data with SNR equal to 33dB and 20dB. In [50], in order to account for the noisy nature of output-only operational vibration data, the authors conducted various tests with different excitation levels and different environmental conditions with the purpose of identifying when a sensor fault occurred. Nonetheless, to the authors' knowledge, there is still no research on extensive studies on noise effects on damage detection with neural networks fed with statistical and subspace-based damage indicators. The main novelties of the current study may be summarized in the following points:

- To avoid complex non-linear structural responses, which may introduce uncontrolled modeling uncertainties introduction, the authors focused on a trivial numerical simply supported beam finite element model in order to effectively study the data corruption effects due to measurements noise;

- A MLP and a one-dimensional convolutional neural network (1D-CNN) network architectures have been employed to evaluate the noise effects on the damage detection task;

- Statistical features and subspace-based damage indicators are the damage-sensitive features that fed up the considered neural models to accomplish the damage detection task;

- Three different noise levels have been defined to better simulate a realistic sensors array placement, resembling real-world sensors characteristics;

- Robustness evaluations have been conducted by considering the neural models trained with data contaminated with a certain noise level, whereas the accuracy performances have been computed with test set data corrupted with different SNR levels.

This document is organized as follows. In section 2, the adopted numerical beam model is presented, followed by a survey of the nowadays most adopted sensors typologies in SHM with corresponding noise levels. In section 3 the damage detection technique based on subspace-based damage indicators is briefly described. In the final part of this section, the neural models adopted in the current study have been illustrated, discussing about the three proposed methods analysed in the current study. Eventually, in section 4, the numerical results are presented and extensively argued, evidencing the robustness of the analyzed neural models with respect to different noise levels.

2. Monitoring simulation with realistic sensors

In this work, the effect of noise on classification performance using deep learning (DL) models is analyzed. In real-world applications, SHM is performed by collecting data through the use of sensors that are unavoidably generating noise errors. Data-driven signal analysis techniques can be strongly affected by the presence of noise in the signals. For this reason, it is essential to define what SNRs are such that classification methods are ineffective. As depicted in Figure 1, in this paper, a numerical beam model has been used to simulate the monitoring data. Different reasonable SNR levels were assumed to simulate actual sensor responses. After simulating the signals affected by the noise, three sets of damage features are extracted to define three different datasets to feed up the neural model classifiers. In case (A), the classification is carried out based on some statistical features estimated from the vibration data. In cases (B) and (C), the dataset is supplemented by the inclusion of subspace-based damage indicators. The effectiveness of using such indicators in detecting structural health state is well-known in the literature [67]. In particular, in case (B), a subspace-based indicator is considered in addition to the statistical feature of the case A. Eventually, case (C) considers an entire set composed of only subspace-based damage indicators. They have been computed by varying the computational parameters required to define the subspace-based damage indicators for the purpose of removing the arbitrary user's choice of these parameters which significantly affects their calculations. More specific details about the datasets of cases (A), (B) and (C) are reported in section 3.2. The classification of signals was then carried out considering the use of two different neural network architectures, i.e. a MLP and a 1D-CNN, for the three above-mentioned datasets.

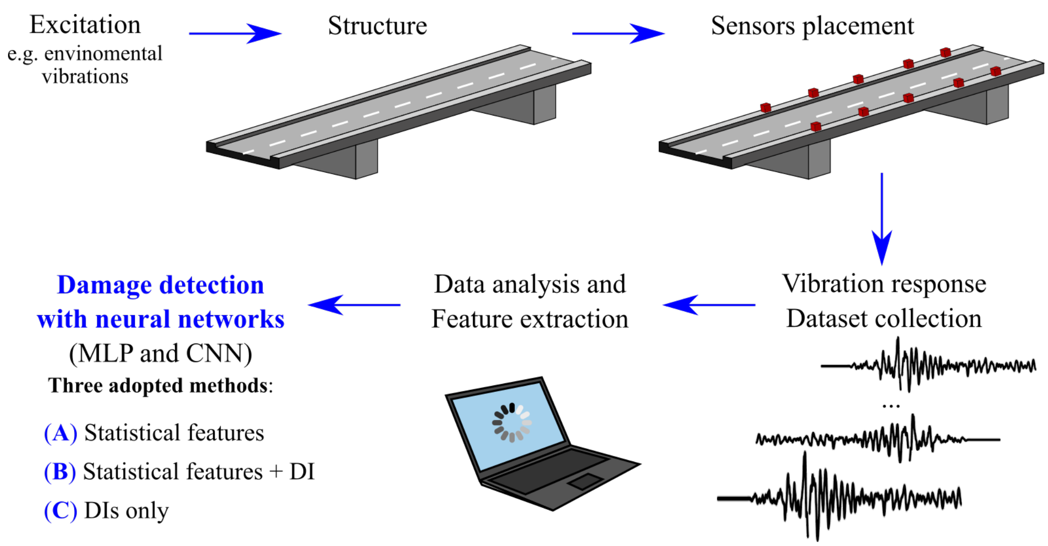

Figure 1: Monitoring and data collection flowchart for the proposed damage detection task with neural networks.

2.1. Numerical beam model and noise-free data collection

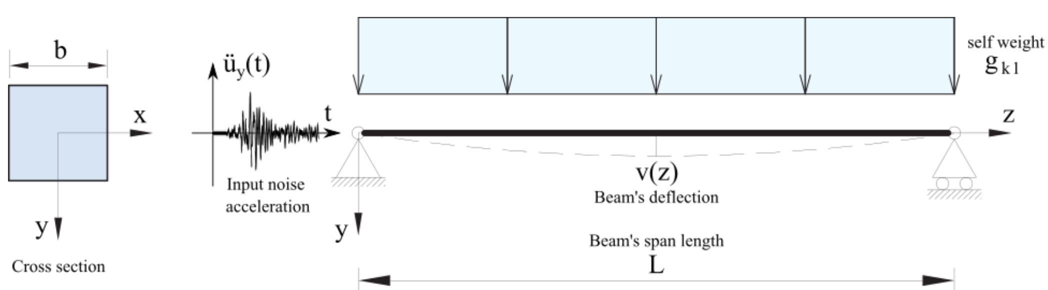

Figure 2: Simply supported beam geometry illustration. x, y, z denotes the Cartesian coordinates reference system, b is the square cross section side, L is the span length, g_{k1} is the self-weight which produces the static deflection $v(z)$. A Gaussian white noise acceleration input ($u_y(t)$) is adopted as dynamic input to the simply supported beam.

The output-only vibration dataset has been obtained with a finite element (FE) modeling of a simply supported beam. The structural model has been chosen as simply as possible for the main purpose of this work, i.e. analyzing the effects of the sensors' noise, thus avoiding some uncontrolled modeling errors will affect the outcomes. The FE model has been implemented with OpenSeesPy module [74]. This tool allows exploiting all the advantages and

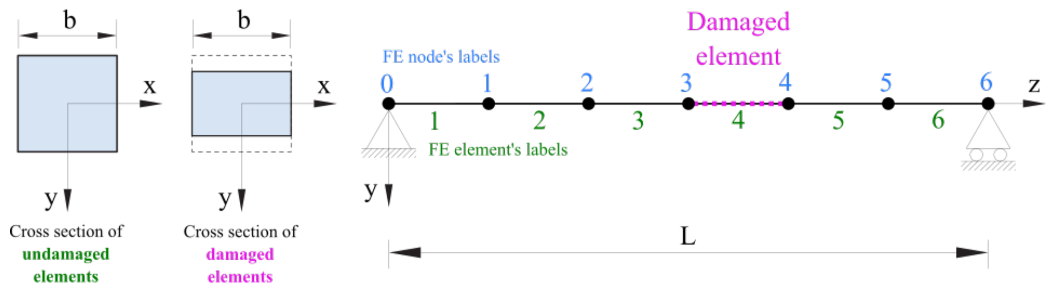

Figure 3: Finite Element (FE) beam model. Damaged elements are modeled with a percentage cross section reduction.

powerful capabilities offered by the open system for earthquake engineering simulation (OpenSees), using a front-end implemented in the python environment instead of the traditional tool command language (Tcl) approach. The simply supported beam has been modelled considering a square cross-section of $0,10m$ and a span length of $2,00m$. The structural material is steel characterized by Young's modulus $E = 210GPa$ and a mass density of $\rho = 7850kg/m^3$.

The beam element has been discretized with a uniform mesh. As illustrated in Figure 3, the meshing is developed by assuming to divide the beam domain into six finite elements. In this way, seven nodes labelled from 0 to 6 are identified in the model. The constraint conditions of the hinged beam are applied to the extremity nodes 0 and 6, which are thus considered fixed in the vertical direction. In the central nodes, 1 to 5, the time history acceleration responses have been collected, simulating a realistic monitoring system with accelerometers placed in correspondence with the nodes as depicted in Figure 3. Although there are several ways to model structural damage [42], in the present study the damage has been introduced in the model as a percentage reduction of the cross-section area corresponding to the damaged elements. The completely undamaged situation has been set as a reference state. Then, the current damage state has been represented by considering three possible different situations. In the foremost current state, the structure may be still completely undamaged, thus the current state corresponds to the reference state. In the second case, a slight damage is introduced by reducing the cross-sectional area by 25%. Finally, in the last case, a 50% reduction of the cross-sectional area is introduced to represent a sever damage condition. For the sake of generality, the number of damaged sections and their location on the beam domain has been randomly selected. Although the introduced damage may appear far higher than the actual values measured on real structures, e.g. for real-world corrosion attacks, at this stage it was decided to study extreme damage cases on a simplified model. Nevertheless, the presented method can be applied to configurations characterized by different levels of damage without loss of generality. The dynamic analysis was carried out by exciting one support of the structure by a Gaussian random white noise acceleration with a sampling frequency of $50Hz$. The white noise process has been generated by a random sampling of a standard normalized zero-mean normal distribution $N(0, 1)$, and rescaled up to $0.01g$ of peak acceleration. The input acceleration has been limited to the vertical direction since a plane beam model is considered [19]. The time history analyses have been conducted with OpenSeesPy python module. The collected acceleration histories response data simulate a monitoring setup composed of accelerometers with a sampling frequency of $500Hz$. Five-minute acquisition duration sessions have been performed on damaged and undamaged models. Because of the randomness of Gaussian distribution, to ensure that all data can be obtained repeatedly, the authors use the concept of seeds in the random module in python numpy module [21]. Finally, to improve the result's accuracy and ensure that enough data is generated to train the DL models, the seed of the random sampling was set from 1 to 5000 to obtain 5000 time history runs.

2.2. Sensor typologies and noise levels

In recent years, a shift of SHM research away from traditional wired methods toward the use of wireless smart sensor networks (WSSN) has been motivated by many attractive features of wireless smart sensors (WSS) [24]. State-of-the-art WSSs offer the promise of wireless communication, onboard computation, low cost, less invasive installation, small size, and performance equivalent to that of their macro-scale counterparts [27]. In general, the SHM outcomes are highly affected by the sensors' performance [49]. Many types of sensors are used for SHM purposes [5]. Nowadays, the most common tendencies are:

1) Fiber optic sensors (FOS);
2) Piezoelectric sensors (PZT);
3) Micro-Electro-Mechanical systems Wireless Sensors (MEMS-WSS).

In Table 2.2 different types of sensors for SHM are compared. Fiber-optic Sensors (FOS) have several advantages, including increased sensitivity,

Table 1: Characteristics comparison of different types of sensors for SHM.

Type	Advantages	Disadvantages	Applications
Fiber Optic	Immune to electromagnetic interference, small size, lightweight, cheap, durable, allows sensor multiplexing.	Temperature sensitive, strain is partially absorbed by the protective layer.	Strain, low-velocity impact damage, cure monitoring.
Piezoelectric	High mechanical strength, operational for a wide frequency range, cheap, small sizes, work in both active and passive sensing methods.	Lengthy cables, difficult signal interpretation.	Acoustic emission: passive sensing method, detection of matrix cracking, fibre–matrix debonding, delamination, fibre breakage, location of damage possible.
Micro Electro-Mechanical System (MEMS) wireless smart sensors (WSS)	Wireless communication, onboard computation low cost, less invasive installation, small size.	Low resolution compared to wired accelerometers used in SHM application.	Wireless sensors are nodes and platforms for autonomous data acquisition.

reduced size and weight, and low-cost [44, 36]. The shortcomings of FOS include the expensive interrogation system, fragility, and the need for several repeaters to boost the signal [60]. The piezoelectric sensor can measure variations in parameters such as acoustic emission [32], temperature, strain, force, pressure, or acceleration. They are able to convert these parameters to a measurable electrical charge [65]. At the same time, they are characterized by very stable mechanical properties under a wide range of temperatures [61]. Shortcomings of this type of sensor include the water solubility of some piezoelectric crystals, temperature sensitivity and the influence of bond layer thickness [61]. For these reasons, sometimes, they are not the best choice when used in exposed environments to climate agents. Wireless sensors are composed of nodes and platforms for autonomous data acquisition. Traditional structural sensors such as piezoelectric can be attached and benefit from their mobile computing and wireless communication elements [33]. Wireless technology has lower installation costs and allows for flexible system configurations [9]. However, battery-powered wireless sensors are still intertwined related to their energy consumption, size, cost, communication range, hardware design, and risk of data loss [14]. In this study, the micro elctro-mechanical system (MEMS-WSS) accelerometer are considered. This type of sensor is among the most widely used in the field of SHM. A summary of the most commonly used MEMS-WSS accelerometers is reported in Table 2.

In typical real-case data acquisition scenarios, recorded signals are char-

Table 2: Summary of typical MEMS- WSS accelerometers used in SHM for bridges [73].

Model	**Interface**	**Noise-Density** $\mu g/\sqrt{\mathbf{Hz}}$	**Voltage Source(V)**	**Sensitivity (V/g)**	**Range(g)**	**BW(Hz)**
SD-1221	Analog	5	5	2.0	±2	0-400
CXL01LF	Analog	70	6-30	2.0	±1	0-50
CXL02LF	Analog	140	6-30	1.0	±2	0-50
AC310-002	Analog	10	9-20	2.0	±2	0-300
LIS2L02AL	Analog	30	3.3	0.66	±2	0-100
LIS2L06AL	Analog	30	3.3	0.66/0.22	±6/±2	0–100
LIS3L02AS4	Analog	50	3.3	0.66	±2	0-50
LIS344ALH	Analog	50	3.3	0.66/0.22	±6/±2	0-1800
SF1500	Analog	0.3	±6-±15	1.2	±3	0-1500
SF1600	Analog	0.3	±6-±15	1.2	±3	0-1500

acterized by the presence of background noise. The noise effect in SHM is also related to intrinsic sensor errors, including sampling frequency, time, and systematic errors of calibration. All these errors can be eliminated to a certain degree [30]. However, some noise components cannot be removed but only attenuated. The presence of these components can affect the accuracy of the information obtained from the recorded output-only vibration signals. In general, the SNR is typically used to define the quality of recorded signals within the SHM paradigm. The accuracy of monitoring data is strongly influenced by this parameter. Generally, the SNR is not a fixed parameter of the sensors and sometimes the actual working conditions of the sensors are relatively harsh, thus it becomes difficult to determine the true SNR parameter. According to Rahaman [48], the current state-of-the-art MEMS sensors can guarantee an SNR that ranges between 27dB and 67dB under real-world working conditions. In this paper, three different level of SNR are chosen to simulate MEMS performance on real-case data collecting: 20dB (low quality), 40dB (medium quality), and 60dB (good quality).

Many researchers use Gaussian white noise to simulate noise-containing samples and to verify the noise reduction effect of the proposed model [49, 71].

Compared to other synthetic noise distributions, Gaussian noise seems to be the best simulation of real noise, especially in the case where the noise source of real noise is particularly complex [18]. According to the maximum entropy theorem of limited power, if the average power is limited when the source conforms to the Gaussian distribution, the source's entropy is the largest. White Gaussian noise is the noise that interferes the most with information if power is assumed to be limited. Based on the assumptions above, synthetic Gaussian noise is an excellent approximate simulation when dealing with this complexity and without knowing the actual noise distribution. Additionally, the design of algorithms and network structures for DL does not strongly depend on the probability distribution of noise [52, 68].

The recorded output-only vibration signal $y(t)$ is composed of two additive parts: the signal itself $x(t)$ and the noise $n(t)$, such as:

$$y(t) = x(t) + n(t) \tag{1}$$

The SNR can be calculated as a function of the ratio between the signal power P_{signal} and the noise power P_{noise}:

$$SNR_{dB} = 10log_{10}\left(\frac{P_{signal}}{P_{noise}}\right) \tag{2}$$

In general, real-world sensors are not able to acquire data continuously but only with a certain sample rate. Thus, a real-case signal is composed of discrete data amplitudes $S = \{S_1^1, S_2^1, ..., S_k^1\}$. Thus, the signal power P_{signal} can be calculated as:

$$P_{signal} = \frac{1}{n}\sum_{k=1}^{n} S_k^2 \tag{3}$$

whereas the power of the noise reads:

$$P_{noise} = \frac{P_{signal}}{10^{\frac{SNR}{10}}} \tag{4}$$

According to [49], the SNR may also be expressed in terms of logarithmic ratio of the signal and noise amplitudes.

3. Subspace-based damage detection

3.1. Brief review of the subspace-based damage indicators

The stochastic subspace identification (SSI) is a widespread time domain method for OMA [45, 22]. The covariance-driven random subspace identification method firstly calculates the block Toeplitz matrix composed of the output covariance sequence. Then, it performs the Toeplitz matrix's singular value decomposition (SVD) to obtain the observability matrix and controllability matrices. Then, it uses the observability matrix to get the dynamic matrix of the system [64]. The SSI method relies on the following state-space representation [31]:

$$x_{k+1} = Ax_k + v_k \tag{5}$$

$$y_k = Cx_k + w_k \tag{6}$$

In equation (5), $x_k \in R^n$ are the states, $A \in R^{n\times n}$ is the state transition matrix. The term v_k represents the expected environmental excitation defined as a Gaussian white noise sequence with zero mean and constant covariance matrix $Q = \mathbb{E}\left(v_k v_k^T\right) := Q\delta\left(k - k'\right)$ with $\mathbb{E}(\bullet)$. Then, in equation (6), $y_k \in R^r$ are the outputs, $C \in R^{r\times n}$ is the observation matrix, the w_k terms indicate the measurement noise. Notice that n represents the system order and r is the number of sensors.

The feature vector is approximately assumed as zero mean normal Gaussian distributed in the reference state (undamaged) which evolves in a nonzero mean when damaged. Residual vector monitoring the relative changes among the damaged state, and the initial reference state. The present study mainly focused on the subspace-based residuals approach. When influenced by noise and changes in input excitation patterns, Subspace residuals are conventional and robust [54]. The residual matrix relies on the orthonormal property between the subspaces related to a reference state in comparison with the subspace related to a noisy or damaged state. Subspace-based residuals approach is based on the covariance-driven output-only subspace identification algorithm. Cross-covariance between the states and the outputs $G = E\left(x_{k+1}y_k^T\right)$ the theoretical output covariances $R_i = E\left(y_k y_{k-i}^T\right) = CA^{i-1}G$ and equation (7) represents the theoretic block Hankel matrix.

$$H_{p+1,q} \stackrel{\text{def}}{=} \begin{bmatrix} R_1 & R_2 & \dots & R_q \\ R_2 & R_3 & \dots & R_{q+1} \\ \vdots & \vdots & \ddots & \vdots \\ R_{p+1} & R_{p+2} & \dots & R_{p+q} \end{bmatrix} \stackrel{\text{def}}{=} \text{Hank}\left(R_i\right) \tag{7}$$

Using measured data $(y_k)_{k=1,\dots,n}$, a consistent estimate $\hat{H}_{p+1,q}$ is obtained from the empirical output covariances:

$$\hat{R}_i = \frac{1}{N}\sum_{k=1}^{N} y_k y_{k-i}^T \tag{8}$$

$$\hat{H}_{p+1,q} = Hank\left(\hat{R}_i\right) \tag{9}$$

Basseville et al. [6] originally proposed a residual function obtained by comparing the system reference state (undamaged) with the current one (damaged or undamaged). The system parameters in terms of eigenvalues and eigenvectors in the reference and current states are denoted respectively Θ_0 and Θ. In OMA SSI-COV method, the modal intrinsic properties information is obtained by the factorization property of the Hankel matrix which allows decomposing it in an observability matrix and a reversed controllability matrix. The observability matrix is thus calculated starting from the Singular Value Decomposition (SVD) of the Hankel matrix:

$$\widehat{H}_{p+1,q} \approx [\boldsymbol{U}_1\boldsymbol{U}_2]\begin{bmatrix} \boldsymbol{S}_1 & \mathbf{0} \\ \mathbf{0} & \mathbf{0} \end{bmatrix}[\boldsymbol{V}_1\boldsymbol{V}_2]^T \approx \boldsymbol{U}_1\boldsymbol{S}_1\boldsymbol{V}_1 \tag{10}$$

U_1 represents the left active subspace of the independent column vectors of the Hankel matrix, whereas U_2 denotes the null subspace of the independent column vectors of the Hankel matrix. Similar definitions are provided for V_1 and V_2 for row vectors of Hankel matrix. Finally, S_1 collects the non-neglectable singular values in a diagonal matrix sorted

$$U_1^T\hat{H}_{p+1,q}V_1 \approx S_1 \tag{11}$$

$$\hat{H}_{p+1,q}\mathbf{V}_2 \approx \epsilon_V \tag{12}$$

$$U_2\hat{H}_{p+1,q} \approx \epsilon_U \tag{13}$$

Residues ϵ_V and ϵ_U can be different from zero vectors because of noise effect or neglected weakly excited high modes. They are not the ideal candidates for tracking relative changes for damage detection purposes. The amplitude of the residues, resulting from the definition of the system order or the amplitude excitation, may mask the residues variation due to minor structural damages. Instead, the above property can be exploited by comparing two different states. Therefore, instead of using the null space $\mathrm{S}\left(\Theta_0^T\right)$ on the parameterized observability matrix, an empirical (nonparametric) null space S is computed on an estimated block Hankel matrix from data in the reference state using e.g., the SVD. The residue is thus expressed in matrix form as:

$$\hat{\epsilon}_c = S^T \hat{H}_{p+1,q} \tag{14}$$

where S^T is the left null space of the block Hankel matrix $\hat{H}_{p+1,q}$ in the reference state and $\hat{H}_{p+1,q}$ is the covariance block Hankel matrix in the current, possible damaged one. From the practical point of view, the excitation covariance Q may vary between different measurement sessions of the system because of random environmental factors, whereas the excitation is assumed to be stationary during one single measurement session. A change in the excitation covariance Q leads to a change in the cross-covariance between states and outputs G and thus in the Hankel matrix. Yan et al. [67] presented an innovative and interesting residual definition, which appears to be robust to variations of the excitation. Let $\hat{U}_1$ be the matrix of the left singular vectors obtained from an SVD of $\hat{H}_{p+1,q}$Since $\hat{U}_1$ is a matrix with orthonormal columns, it is independent of the excitation Q. Therefore, the residual matrix can be written as

$$\hat{\epsilon}_r = S\hat{U}_1^T \tag{15}$$

Yan et al. [67] provided a geometrical interpretation of the residual matrix concept, such as the expression of a loss of orthonormality between reference subspace and another current state. Therefore, they give some damage indicators related to the rotation angle between the two subspaces when structural damage occurs. Finally, they established that the norm of matrix gave the best-found damage indicator $\hat{\epsilon}_r$

$${\hat{\sigma}_N}^2 = norm \ \ (\hat{\epsilon}_r) \tag{16}$$

where norm ($\bullet$): $R^{m \times n} \rightarrow R$ denotes the matrix spectral norm operator which corresponds to the maximal singular value of a matrix, from the numerical point of view. Therefore, the authors adopt the following damage indicators:

$$I_{y,nr} = norm\,(\hat{\epsilon}_c) \tag{17}$$

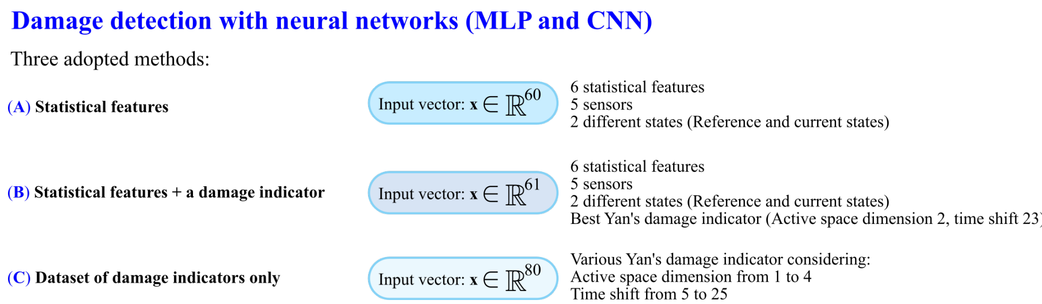

Figure 4: Summary of the three adopted methods (A), (B), and (C) with the definition of the input vectors to feed the neural models in the three analyzed cases.

$$I_{y,r} = norm\left(\hat{\epsilon}_r\right) \tag{18}$$

In the current study, the Yan's et al subspace-based damage indicator definition has been selected as a damage-sensitive feature to train the neural classification models presented in the next section.

3.2. Neural models and datasets (A), (B) and (C) description

The main goal of the present work is to analyze the noise effects of an AI-based health state classifier based on the accelerogram time histories recorded by the simulated beam monitoring system. The problem is a multi-class classification problem of the current health state of the structural system. The completely undamaged situation has been set as a reference state. On the other hand, three possible states has been defined in section 2 for the current state: undamaged, slightly damaged, and severely damaged. 5000 time history responses have been collected from the simulated monitored beam under environmental excitation. These time series responses have contaminated by additive Gaussian noise to simulate real-world MEMS sensors, defining three SNR levels: 20dB (low quality sensors), 40dB (medium quality sensors), and 60dB (good quality sensors). Referring to the data-driven SHM paradigm, DL techniques appear naturally suited to accomplish the health states classification problem [29, 62]. Specifically, in this work, two different neural models have been used to perform the classification problem, always considering three different input datasets denoted as case (A), (B) and (C). As illustrated in Figure 4, the datasets are obtained by considering some statistical features extracted by the acquired signals from each sensors and also accounting for the Yan's et al. damage indicators, reviewed in section 3.1. The dataset (A) is based on 6 statistical features computed from the acquired signals obtained by each sensor, both in the reference and in the current state. As demonstrated in [13], the statistical features in equations (19)-(26) appear to be the most effective ones if considered by a machine learning model adopted to time series for SHM applications. Considering both acceleration time series recordings x, the extracted features are the peak value $x_{P,(i,j)}$, the mean square value $x_{MS,(i,j)}$, the root means square $x_{RMS,(i,j)}$, the variance $x_{VAR(i,j)}$, the standard deviation $x_{STD,(i,j)}$, the skewness $x_{Skew,(i,j)}$, the kurtosis $x_{Kurt(i,j)}$ and the K-factor $x_{K,(i,j)}$.

$$x_{P(i,j)} = max \left\{ |x_k| \right\}_{k=1}^{n} \tag{19}$$

$$x_{MS(i,j)} = \frac{1}{n} \sum_{k=1}^{n} x_k^2 \tag{20}$$

$$x_{RMS(i,j)} = \sqrt{\frac{1}{n} \sum_{i=1}^{n} x_k^2} \tag{21}$$

$$x_{VAR(i,j)} = \frac{1}{n} \sum_{k=1}^{n} \left(x_k - \bar{x} \right)^2 \tag{22}$$

$$x_{STD,(i,j)} = \sqrt{\frac{1}{n} \sum_{k=1}^{n} \left(x_k - \bar{x} \right)^2} \tag{23}$$

$$x_{Skew,(i,j)} = \frac{1}{n} \sum_{k=1}^{n} \left(\frac{x_k - \bar{x}}{x_{STD,(i,j)}} \right)^3 \tag{24}$$

$$x_{Kurt(i,j)} = \frac{1}{n} \sum_{k=1}^{n} \left(\frac{x_k - \bar{x}}{x_{STD,(i,j)}} \right)^4 \tag{25}$$

$$x_{K,(i,j)} = x_{P,(i,j)} \cdot x_{RMS,(i,j)} \tag{26}$$

In the equations (19)-(26), k is the component of the time series vector x, which is composed of n elements, i denotes the number of the simulation out of the 5000 total runs, and j denotes the accelerometer from which the time series has been recorded. Considering an acquisition time interval of five minutes for each run, a sampling frequency of $500Hz$, and 5 accelerometers installed for each beam, n results to be equal to 150000 samples. For each simulation acquisition, the extracted features considered in the dataset

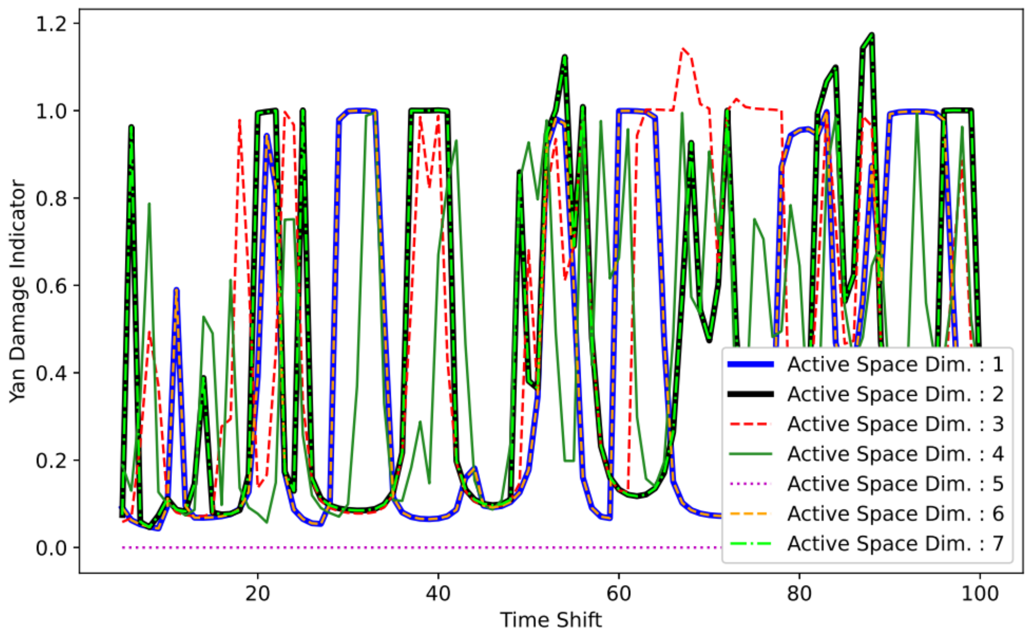

Figure 5: Empirical sensitivity analysis on active space dimensions, compared with various time shift imposed by the user.

(A) are the peak value $x_{P,(i,j)}$, the root mean square $x_{RMS,(i,j)}$, the variance $x_{VAR(i,j)}$, the skewness $x_{Skew,(i,j)}$, the kurtosis $x_{Kurt(i,j)}$ and the K-factor $x_{K,(i,j)}$. These six statistical features have been extracted from each sensor producing, in total, 30 extracted features. For each simulation, two damage conditions have been considered (reference and current state). Altogether, a total of 60 features have been produced as input from each algorithm run.

The dataset (B) includes the same features as the dataset (A) with the addition of an optimal Yan's indicator. Thus, the input vector to feed the neural models has in total 61 components. Figure 5 displays a significant variation among the Yan et al. subspace-based damage indicator by considering different active subspace dimensions and time shifts. The active space dimension is related to the left singular column vectors with non-zero singular values. Focusing on a specific time shift, the Yan et al. indicator value differs among the considered active space dimensions. The time shift is related to the block rows considered in the block Toeplitz matrix assembling. According to [49], to identify the system order n, the relationship $li \geq n$ must be respected, where l is the number of sensors and i the number of

Table 3: Summary of the properties of the implemented CNN.

Layer	Output Shape	Activation Function	Parameters Number
Input and reshape layer	[(None,80,1)]	-	0
Conv1D_1	(None,77,15)	ReLU	75
Conv1D_2	(None,74,15)	Batch Normalization +ReLU	(915+60)
Max Pooling	(None,24,15)	-	0
Conv1D_3	(None,21,40)	Batch Norimalization +ReLU	(2440+160)
Global Average Pooling	(None,40)	Drop out	0
Output Dense Layer	(None,3)	Softmax	123

Total Trainable parameters: 3773
Trainable parameters:3663
Epochs: 1000
Loss: Categorical Cross-entropy (Optimizer: Adam)

block rows, i.e. the time shift. In the literature, a reasonable choice for the time shift is often related to the power spectral density matrix [49]. Figure 5 shows that the results of active space dimension 1 are almost the same as dimension 6, whereas the results of dimension 2 are the same as dimension 7. Indeed, the results of this initial sensitivity analysis suggested adopting an active space dimension equal to 2, which is consistent with the higher non-zero singular values. For this reason, the active space dimension equal to 2 and the time shift equal to 23 are selected. This choice allows mitigation of the computational effort. Finally, in the dataset (C) only Yan et al. damage indicators have been considered. They have been computed considering various time shifts from 5 to 25 and truncation orders, which define active space dimensions, from 1 to 4, collecting in total 80 features for each simulation of the all 5000 time history runs.

In this paper, two artificial neural network architectures have been implemented for each dataset previously described. In particular, a one-dimensional convolutional neural network (1D-CNN) and a multi-layer perceptor (MLP) have been trained. The 1D-CNNs are used in this work because of their effectiveness in obtaining a feature maps from a short segment of the overall dataset, especially in the case in which the feature's location in that data

Table 4: Summary of the properties of the implemented MLP

Layer	Output Shape	Activation Function	Parameters Number
Input and reshape layer	[(None,80)]	-	0
Hidden layer	(None,15)	ReLU	930
Output Dense Layer	(None,3)	Softmax	48

Total Trainable parameters: 3773
Trainable parameters:3663
Epochs: 1000
Loss: Categorical Cross-entropy (Optimizer: Adam)

segment is not highly correlated. The CNN model has been implemented in python through the TensorFlow module with the Keras front-end [10]. In Table 3 the parameters of the CNN model used on dataset (C) are reported, since it is the most complex and representative case.

Even the MLP model has been implemented in python through the TensorFlow and Keras modules [10]. Table 4 introduces the model trained on the dataset (C) (see also Figure 6), which is the most complex and representative. The MLP presents a single hidden layer with 15 units and an output layer composed of three units, since three possible damage scenarios have been envisaged. In this MLP architecture, the softMax activation function has been adopted. This particular function forces the output vector prediction to sum up to one. Therefore, the output value will represent the probability of each input vector to belong to a certain envisaged damage scenario. The loss function is a metric used to judge the model's performance. The categorical cross-entropy loss function is the most widespread in multi-class classification tasks to quantify the difference between the output classes probability distributions. The optimization algorithm iteratively updates the neural weights of the various units in order to minimize the loss function within the back-propagation process. In this case, the most widespread Adam algorithm has been used. This is an effective stochastic optimization method that requires only a small amount of memory and only requires first-order gradients. It is an excellent adaptive learning optimizer under default working conditions.

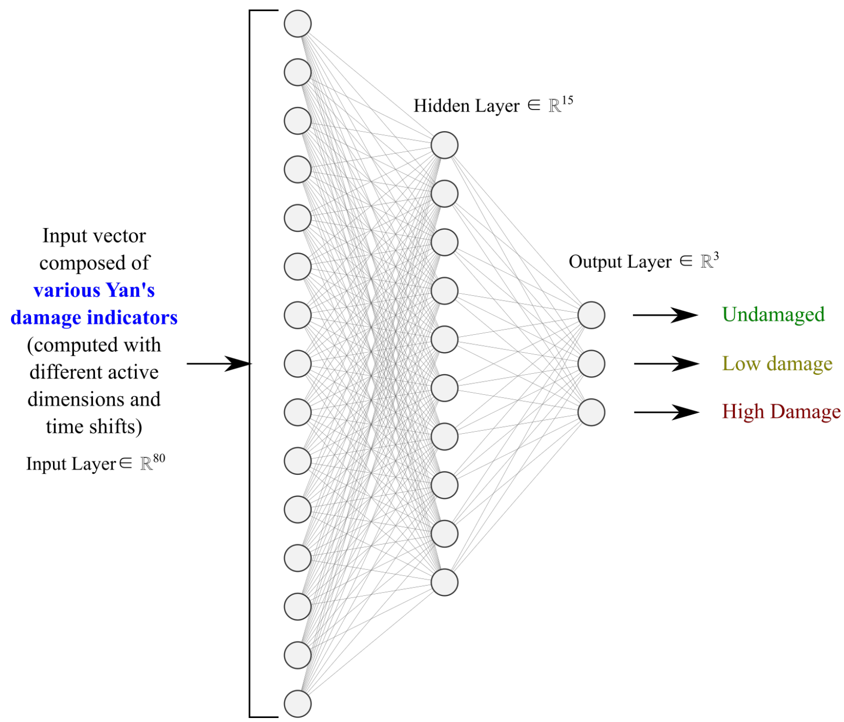

Figure 6: Schematic model of MLP architecture for case (C).

4. Numerical results and discussion

The three datasets (A), (B), and (C) have been computed under different SNR conditions to investigate how the level of noise affects the three-class classification problem. Prior to train the neural models, the dataset is divided into two parts: a training set and a test set, with proportions of 80% (4000 simulations) and 20% (1000 simulations) respectively. The test set allowed testing the trained model's predictive capabilities to evaluate generalization error [51]. A further partition of 10% inside the training set defined the validation set for assessing accuracy performance online during the training phase among the epochs.

4.1. MLP and CNN Multiclass Classification Results

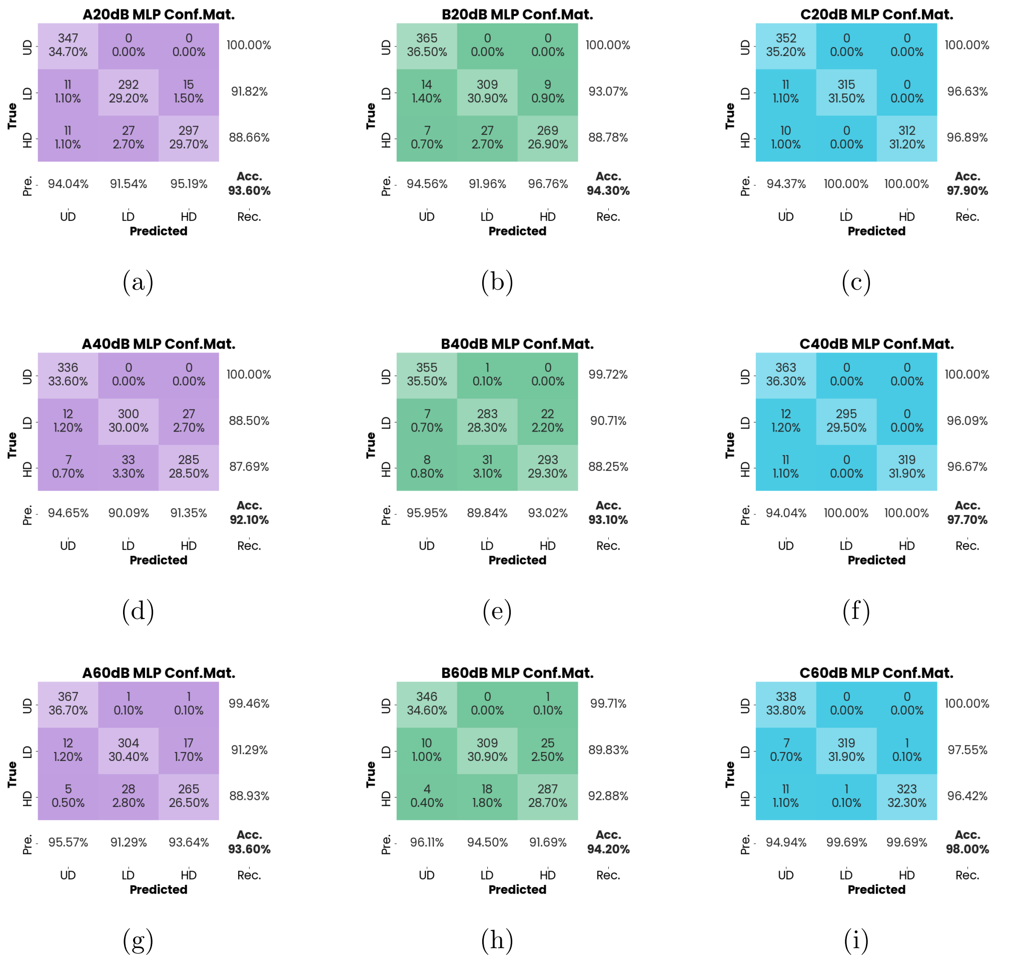

Figure 7: classification results of the MLP models.

The performance of the best trained MLP model on different SNR levels has been validated with the test set, whose classification results have been condensed in the confusion matrix illustrated in Figure 7. On the other hand, Figure 8 shows the results from the best CNN model on the same datasets. The accuracies are all above 90% for MLP models but decrease to 82.80% for CNN models in the cases (A) and (B). Accuracy measures the portion of the test set which has been correctly classified.

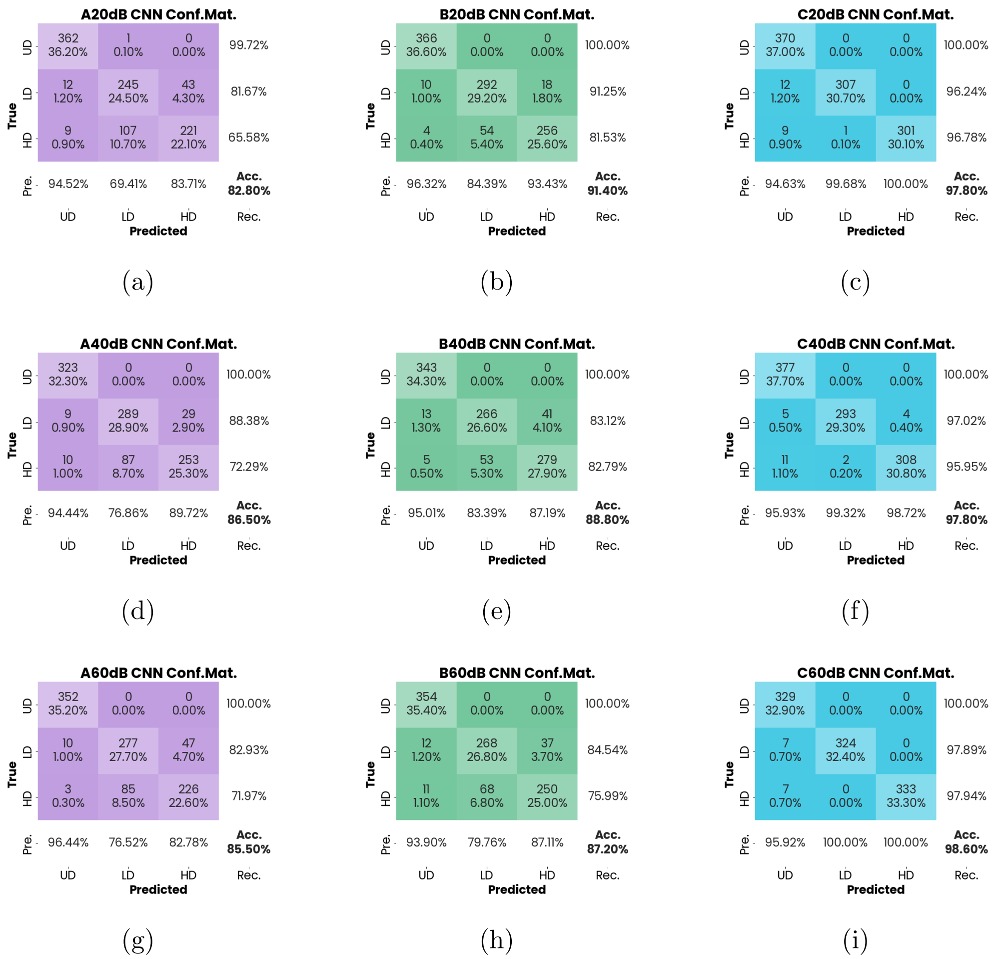

Figure 8: Classification results of the CNN models.

The precision measures the number of samples correctly classified in a particular class over the total number of samples which have been associated with that class. In contrast, the recall represents the number of samples correctly classified into a specific class over the number of samples which belongs to that class [51]. The precision and recall values are quite high, being above the 87.69% for all the classification possible outcomes in MLP models. Instead, there is a significant decrease on CNN, even to 65.58%. Considering CNN models in 60dB SNR levels, in Figure 8 (g), the overall accuracy for method (A) is 85.50%. Figure 8 (h) shows that the accuracy for method

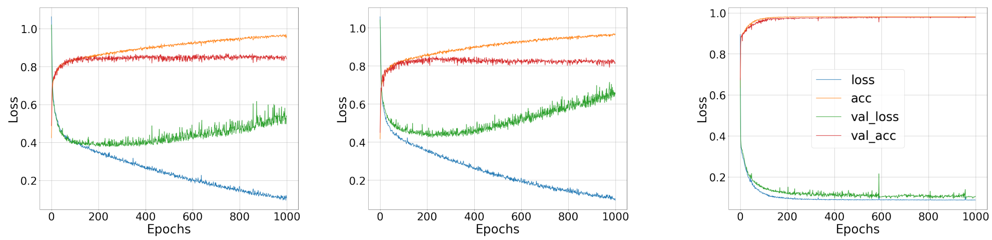

(a) (b) (c)

Figure 9: 60-dB noise level CNN training performances history during the epochs.

(C) is around 87.20%, and the higher classification of the method (B) with respect to method (A) proves that this most informative subspace-based feature improves the classification performances of both CNN and ANN model for every noise levels. In Figure 8 (i), the final accuracy for the trained model in method (C) is 98.60%. The outstanding higher classification performance of method (C) to methods (A) and (B) proves that considering an entire set of informative subspace-based features improves the classification performances of the DL models for the damage detection task.

Best weights and models should be saved for prediction. The loss function both for the training and the validation sets is depicted over the epochs, for the CNN model in 60dB SNR levels is reported in Figure 9. When the validation loss starts to increase after a monotonic decreasing behavior, the overfitting of the model is reached. In Figure 9 (a), the validation loss increases gradually while the loss on the training set decreases, reaching the overfitting point at around 400 epochs. The same situation appears in Figure 9 (b), while the overfitting point is around 450 epochs. The validation accuracy continues to increase a little biteven when the overfitting point is reached. In Figure 9 (c), the loss is relatively low. From a deeper insight into the loss and accuracy trends, it would virtually be possible to stop the training to epoch 150 to save computational cost and obtain almost the same performances.

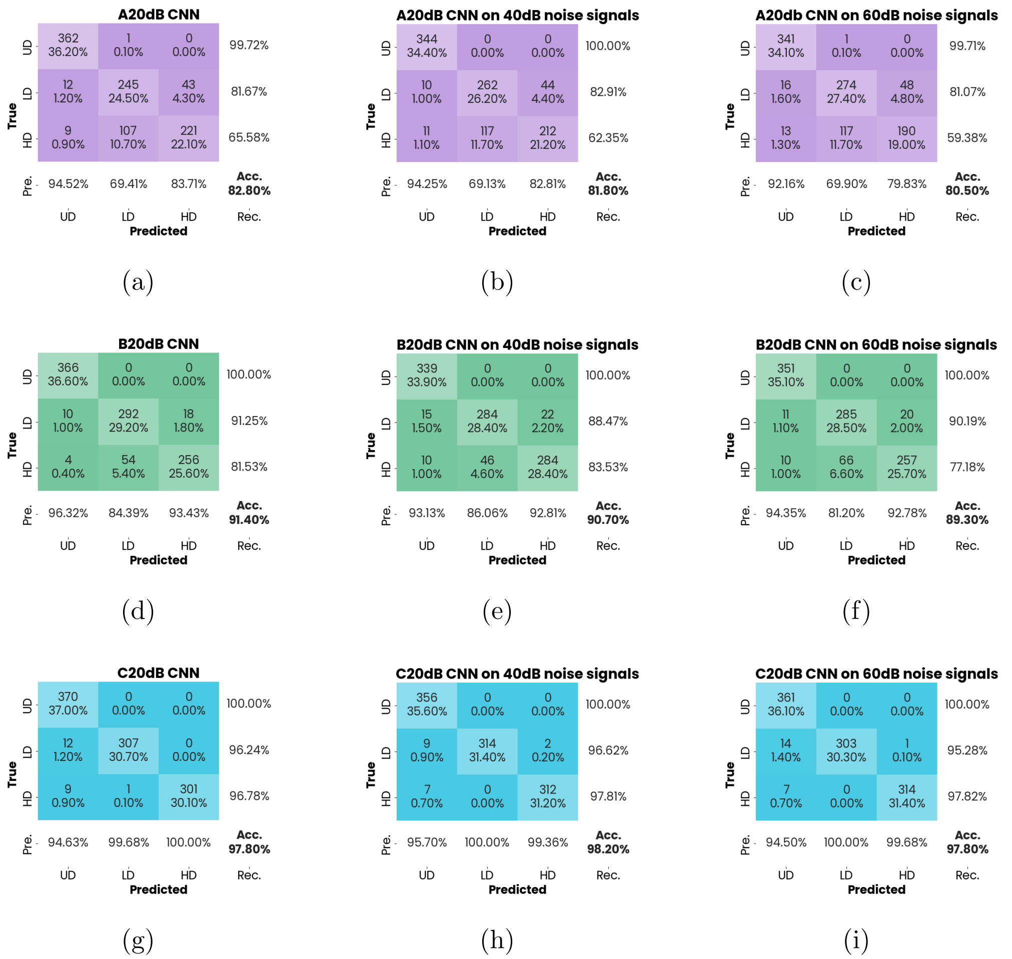

Figure 10: Classification results of the 20dB CNN models on other SNR levels in all three methods.

The robustness of the deep-learning is affected by the noise. Figure 10 (a), (d), and (g) respectively show the performance of the best CNN models in methods (A), (B), and (C). In method (A), the performances of the CNN model trained with the 20dB SNR level have been validated with the test set from 40dB SNR level, as illustrated in Figure 10 (b). The overall accuracy obtained results to be 81.80%. In Figure 10 (c), accuracy is 80.50% for the test set with the 60dB SNR level. The same outcomes can be drawn even for methods (B), and (C). Figure 11 shows the results for 60dB noise levels.

Even if the noise level has changed significantly, the previously trained model gives good predictions.

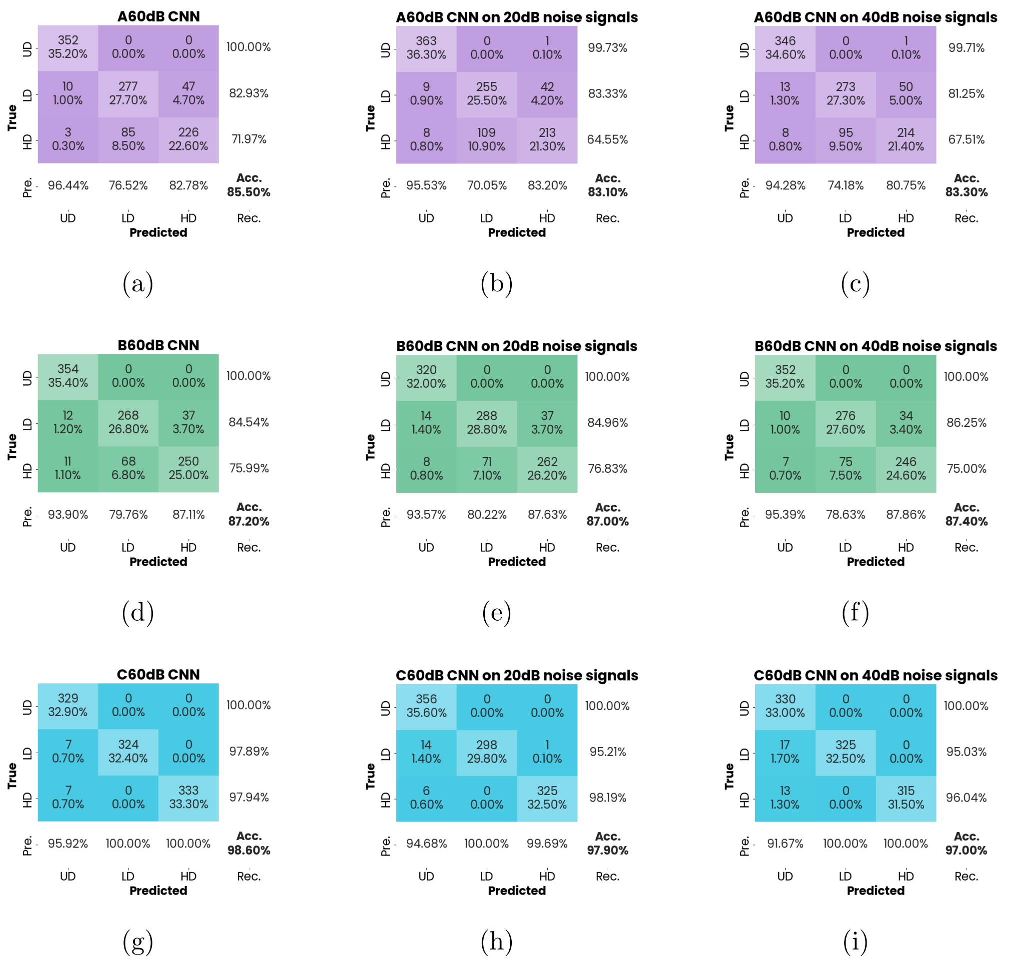

Figure 11: Classification results of the 60dB CNN models on other SNR levels in all three methods.

The current MLP and CNN models can provide quite interesting multi-class classification results considering the statistical time series features coupled with the Yan et al. subspace damage indicator. This allows extending the capabilities of the MLP model. Furthermore, a good generalization of the current DL models is related to the fact that the 5000 numerical simulations randomly considered both how many damaged elements to consider and the level of damage to associate with those selected elements. This produced a time-series signal which covers many different cases, which was anyway successfully traced back to the three possible classification results: undamaged situation, low damage status (cross-section reduction of about 25%) and high damage condition (cross-section reduction of about 50%). The influence of noise is further reduced. DL models are robust to noise.

4.2. Comparisons between different features

In Figure 12, the bar graph compares the overall accuracy of the three different datasets for both the applied ANN.

These results are retrieved from the numerical beam method which enables performing a novel and extensive empirical sensitivity analysis on parameters that affect the subspace-based damage indicators, even considering the noise that may affect a real-world method. For CNN models in Figure 12 (b), method (A) leads to an accuracy of 85.50%. The accuracy increases to 87.20% by considering method (B). This most informative indicator was obtained by setting the optimal parameters from the results of the empirical sensitivity analysis in Figure 5. This improvement is observed in every presented methods (Figure 7 and Figure 8). Outstanding accuracy has been obtained with method (C), which reaches about 98.60%. It considers as an input dataset many subspace-based damage indicators only, removing the user's arbitrary choice on the parameters to be taken into account. Therefore, this last proposed method (C) represents the most useful approach to effectively address the damage detection task. Further comparisons have been performed in terms of recall and precision as illustrated in Figure 13. Focusing on the recall metric, for every of the considered methods the undamaged structures have been correctly classified more than 90% of the times. Method (C) reaches the highest recall both in low damage and high damage classes with values higher than 97.94%. This shows the advantages to consider the subspace-based damage indicator with respect to the statistical features alone. On precision metric, remarkable precision values have been obtained in method (C) for which 100% have been reached for low damage and high damage in CNN models. The CNN models have probably learned optimal weights to effectively reconduct low and high damage methods.

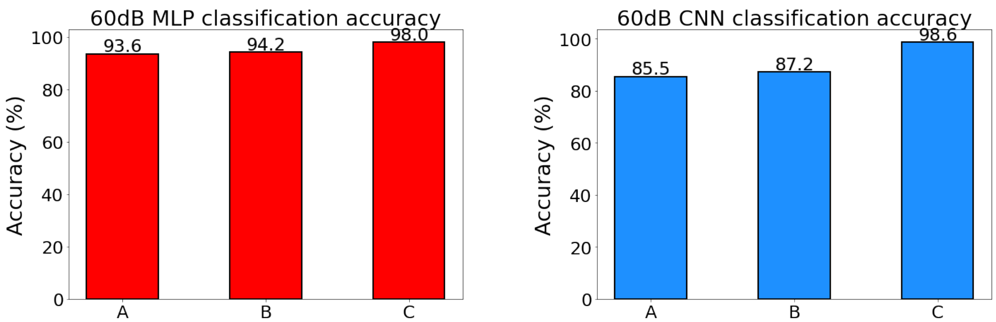

(a) (b)

Figure 12: 60dB models classification comparisons on accuracy among the proposed methods (A), (B), and (C)

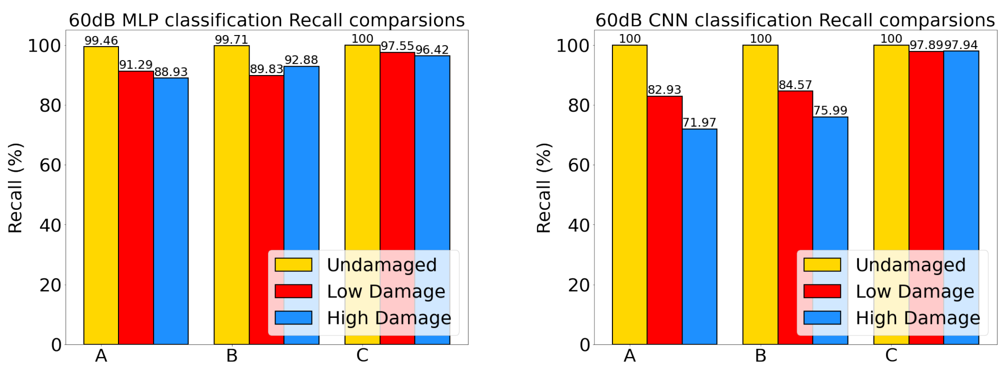

(a) (b)

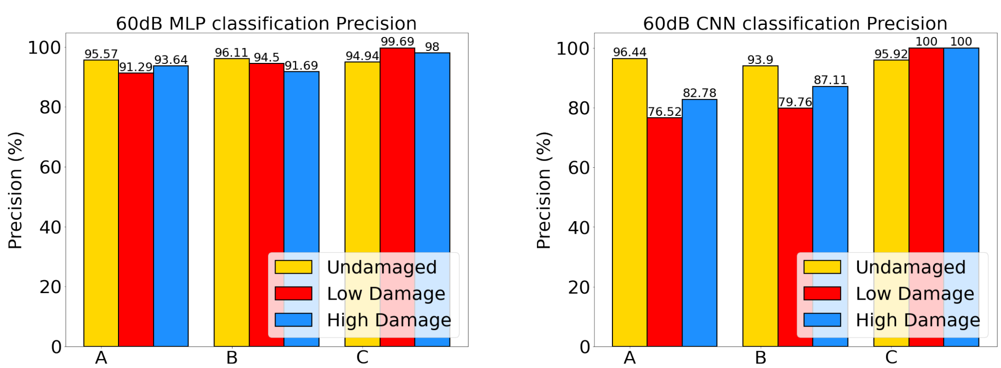

(c) (d)

Figure 13: 60dB models classification comparisons on Recall and Precision among the proposed methods.

4.3. Comparison between CNN and MLP models

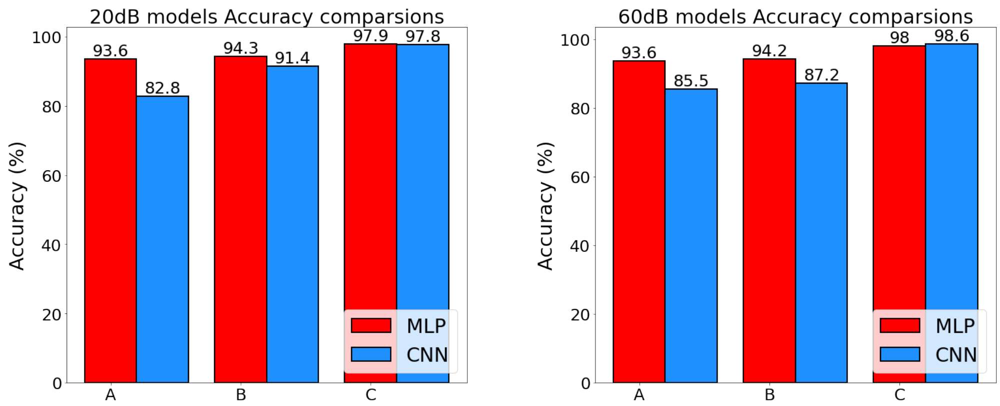

(a) (b)

Figure 14: 20dB and 60dB models classification comparisons on accuracy among the proposed methods.

Figure 14 shows the comparison between the CNN model and the ANN model. Considering the 60dB models, from Figure 14 (b), the accuracy of the CNN model in method (A) is 85.5%, resulting to be lower than 93.6%, the accuracy of MLP model. The same behavior is observed in method (B), where the accuracy decreased from 94.2% in MLP to 87.2 in CNN model. In methods (A) and (B), discrete statistical features are used. Consequently, the fully connected layers of the MLP may be better to deal with these features than the convolution kernel of CNN. In any case, a very impressive accuracy is shown for method (C). The accuracy of MLP reached 98%, while the accuracy of CNN is even higher being 98.6%. This also proves the effectiveness of Yan's et al. damage indicators in SHM for realistic sensor datasets. The same results have been obtained for 20dB and 40dB models. CNN model seems to perform worse, as well as MLP, on methods (A) and (B). The main differences occur in distinguishing the degree of damage. Both MLP and CNN perform well in method (C) with different noise levels. Yan's damage indicator is an effective indicator even considering different noise levels and different DL models.

4.4. Noise effects final overview

Figure 15 illustrate the influence of different noise levels on three analyzed methods. For CNN architecture in method (A), the final accuracy on

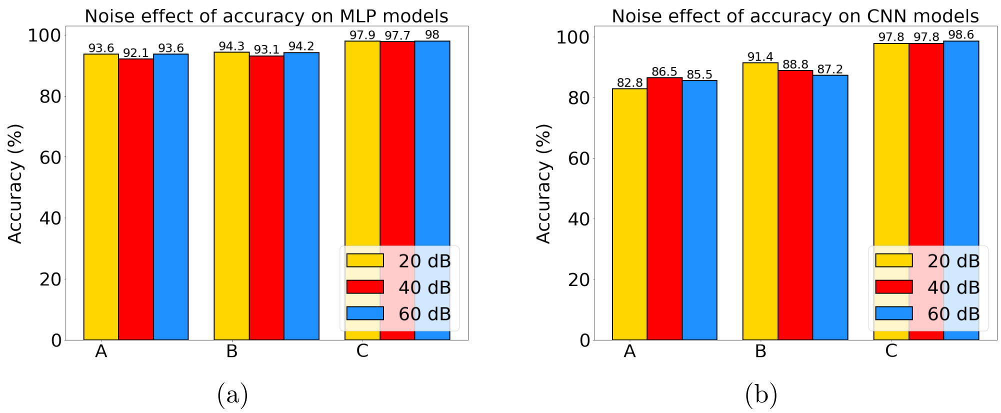

Figure 15: 20dB, 40dB and 60dB models classification comparisons on accuracy among the proposed methods.

20dB SNR level is 82.8%, while on 40dB is 86.5%, and 85.5% on 60dB. Considering the three different SNR levels, the outcome is 91.4%, 88.8%, and 87.2% respectively on method (B). Even better outcomes are registered for method (C), being for the three SNR levels equal to 97.8%, 97.8%, and 98.6% respectively. There are indeed fluctuations in the results, but actually, no significant difference between the outcomes from three different noise levels in any method are registered, for both CNN and MLP model. It can be concluded that for realistic sensors, Yan's et al. damage indicator is still an effective indicator in SHM. Also, Figure 15 shows that methods based on Yan's et al. damage indicators and DL models are characterized by robustness to noise. In this work, whether it is low noise level or very high noise level, using DL tools under different feature conditions reliable results are obtained. In addition, the SSI method directly processes and analyzes the response data of the structure in the time domain. It relies on the theory of spatial projection to eliminate the noise signals that are not related to the response data. It also shows good ability to resist noise disturbance. Between the three methods (A), (B), and (C), Yan's et al. damage indicator has the best performance on the accuracy, regardless of noise levels and DL models. As shown, in method (C), every classification accuracy is higher than 98%.

Figure 16 shows the performance of the best model trained with the highest noise condition (60dB SNR level) and the lowest noise condition (20dB SNR level) in dealing with signal characterized by other noise levels.

Considering the result of the 20dB model, reported in Figure 16 (a), it

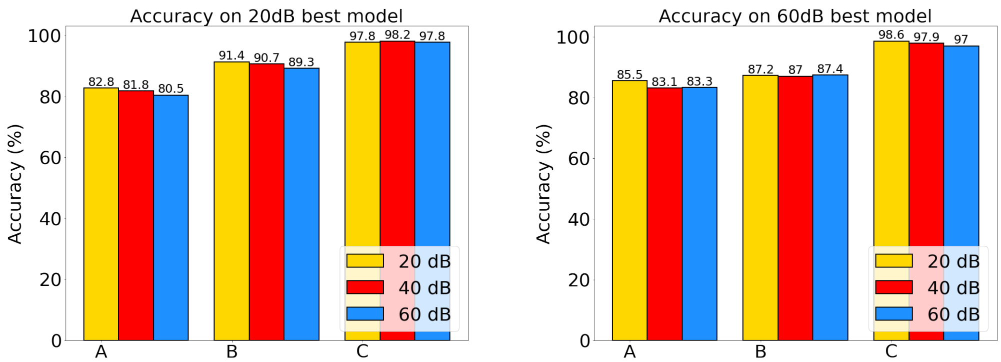

(a) (b)

Figure 16: Accuracy on different SNR levels of the CNN models trained from 20dB and 60dB SNR levels.

results that, in method (A), the 20dB SNR level trained model obtained the highest classification accuracy 82.8% at 20dB SNR level, as expected. The same model tested on signals with 40dB SNR level shows a reduction of only 1% of the accuracy, obtaining 81.8%. The test carried on 60dB SNR level signal results in a further slightly decreasing of the accuracy that results to be equal to 80.5%. The same results are also obtained for methods (B) and (C). Furthermore, the same test is performed using as a training set the signals characterized by an SNR level equal to 60dB (Figure 16 (b)). In this case, the best model has nearly the same performance at different signal-to-noise levels. This result is very meaningful. This research is based on the data obtained from the previously simulated beam model and used to approximate the real-world noise effect. In theory, for different working environments, retraining the models every time based on the collected data the best results can achieve. However, in practice, retraining the models will take a long time and higher costs. In addition, in the real-case scenario, although the error of the sensor changes slowly, the environmental noise changes rapidly. For example, in the real working environment of a bridge, there may be a large change in the SNR within a period with the change in the flow of people, the flow of vehicles, and time. Therefore, the presented method can be generalized and applied to real case studies, as the robustness of the analyzed models has been proven.

5. Conclusions

In the current study, three different damage detection methods (A), (B), and (C) have been proposed to achieve the SHM paradigm level 1, based on statistical features and subspace-based damage indicators. The proposed methods have been accomplished with two DL-based three-classes classifiers, i.e. a MLP and a 1D-CNN. The health state classification is based on datasets obtained by vibration data collected simulating in OpenSeesPy a FE beam monitoring system under environmental dynamic excitation, thus providing noise-free vibration data. The main goal of this study is to provide for the first time an extensive study of the noise effects on DL-based health state classifiers and explore their robustness with respect to different noise levels. Therefore, the noise-free data have been contaminated by an additive stochastic Gaussian noise process calibrated on three SNR levels in order to resemble real-world MEMS sensors. The first damage detection method (A) is based on statistical features calculated on noisy time series data, whereas the second method (B) attempts to enhance the classification performance by adding a more informative damage-sensitive feature, i.e. the Yan's et al. [67] subspace-based damage indicator. The third method (C) represents an innovative solution to the arbitrary definition of the parameters that affect the computation of subspace-based damage indicators. The results obtained from different SNR levels demonstrated that the proposed methods can be generalized to real-world cases. In conclusion, numerically training DL models may provide a robust and almost reliable health state classification system even in the presence of an actual best or worst-case noise situation with respect to the simulated one. The obtained models were apparently able to recognize hidden patterns within output-only multivariate time series noisy vibrations considering statistical and/or damage-sensitive features from all sensor acquisitions simultaneously. Finally, the authors concluded that the analyzed 1D-CNN and MLP models could represent an interesting and valuable first-level anomaly detection to distinguish between an undamaged or reference situation and a possible current damaged one, even if in real-world cases the damage scenario is often unknown. The advantage also lies in the fact that the task can be performed only by recalling the trained model, which is, therefore, faster in-service conditions. Additionally, the trained models appeared effective at any reasonable level of SNR and can achieve optimal performance due to the robustness of the best machine learning models. Future promising research paths may investigate the effectiveness of the proposed methodology with more compact neural networks, such as MobileNet or similar architectures able to be effectively executed in real-time on emerging small electronic edge devices. Further research should explore the proposed methods in SHM anomaly detection in real-world case studies, or even extend the proposed subspace-based indicators also to the other deep levels of the SHM paradigm.

6. Data availability statement

The data that supports the findings of this study are available from the corresponding author upon reasonable request.

7. Declaration of Competing Interest

The authors declare that they have no known competing financial interests or personal relationships that could have appeared to influence the work reported in this paper.

References

[1] Aloisio, A., Pasca, D.P., Battista, L., Rosso, M.M., Cucuzza, R., Marano, G., Alaggio, R.: Indirect assessment of concrete resistance from fe model updating and young's modulus estimation of a multi-span psc viaduct: Experimental tests and validation. Elsevier Structures **37**, 686–697 (01 2022). https://doi.org/10.1016/j.istruc.2022.01.045

[2] Avendaño-Valencia, L.D., Fassois, S.D.: Gaussian mixture random coefficient model based framework for shm in structures with time–dependent dynamics under uncertainty. Mechanical Systems and Signal Processing **97**, 59–83 (2017), special Issue on Surveillance

[3] Balmes, E., Basseville, M., Mevel, L., Nasser, H., Zhou, W.: Statistical model-based damage localization: A combined subspace-based and substructuring approach. Structural Control and Health Monitoring: The Official Journal of the International Association for Structural Control and Monitoring and of the European Association for the Control of Structures **15**(6), 857–875 (2008)

[4] Barrias, A., Casas, J.R., Villalba, S.: A review of distributed optical fiber sensors for civil engineering applications. Sensors **16**(5), 748 (2016)

[5] Barrias, A., Casas, J.R., Villalba, S.: A review of distributed optical fiber sensors for civil engineering applications. Sensors **16**(5) (2016)

[6] Basseville, M., Abdelghani, M., Benveniste, A.: Subspace-based fault detection algorithms for vibration monitoring. Autom. **36**, 101–109 (2000)

[7] Bernagozzi, G., Ventura, C.E., Allahdadian, S., Kaya, Y., Landi, L., Diotallevi, P.P.: Output-only damage diagnosis for plan-symmetric buildings with asymmetric damage using modal flexibility-based deflections. Engineering Structures **207**, 110015 (2020). https://doi.org/https://doi.org/10.1016/j.engstruct.2019.110015, https://www.sciencedirect.com/science/article/pii/S0141029619314476

[8] Brincker, R., Ventura, C.E.: Introduction to Operational Modal Analysis. John Wiley & Sons, Ltd (2015). https://doi.org/https://doi.org/10.1002/9781118535141

[9] Carpinteri, A., Lacidogna, G., Manuello, A., Niccolini, G.: Acoustic emission wireless transmission system for structural and infrastructural networks. In: 8th Internation Conference on Fracture Mechanics of Concrete and Concrete Strucures (2013)

[10] Chollet, F., et al.: Keras (2015), https://github.com/fchollet/keras

[11] Das, S., Saha, P., Patro, S.: Vibration-based damage detection techniques used for health monitoring of structures: a review. Springer Journal of Civil Structural Health Monitoring **6**, 477–507 (2016). https://doi.org/https://doi.org/10.1007/s13349-016-0168-5

[12] Farrar, C.R., Worden, K.: Structural health monitoring: a machine learning perspective. John Wiley & Sons (2012)

[13] Finotti, R.P., Cury, A.A., Barbosa, F.d.S.: An shm approach using machine learning and statistical indicators extracted from raw dynamic measurements. Latin American Journal of Solids and Structures **16** (2019)

[14] Gao, S., Dai, X., Liu, Z., Tian, G., Yuan, S.: A wireless piezoelectric sensor network for distributed structural health monitoring pp. 1–6 (2015)

[15] Gardner, P., Bull, L., Gosliga, J., Poole, J., Dervilis, N., Worden, K.: A population-based shm methodology for heterogeneous structures: Transferring damage localisation knowledge between different aircraft wings. Mechanical Systems and Signal Processing **172**, 108918 (2022)

[16] Gatti, M.: Structural health monitoring of an operational bridge: A case study. Engineering Structures **195**, 200–209 (2019). https://doi.org/https://doi.org/10.1016/j.engstruct.2019.05.102, https://www.sciencedirect.com/science/article/pii/S0141029618336563

[17] Gautier, G., Serra, R., Mencik, J.M.: Roller bearing monitoring by new subspace-based damage indicator. Shock and Vibration **2015** (2015)

[18] Goyal, B., Dogra, A., Agrawal, S., Sohi, B.S., Sharma, A.M.: Image denoising review: From classical to state-of-the-art approaches. Inf. Fusion **55**, 220–244 (2020)

[19] Groth, E.B., Clarke, T.G.R., Schumacher da Silva, G., Iturrioz, I., Lacidogna, G.: The elastic wave propagation in rectangular waveguide structure: Determination of dispersion curves and their application in nondestructive techniques. Applied Sciences **10**(12) (2020)

[20] Gupta, M., Khan, M.A., Butola, R., Singari, R.M.: Advances in applications of non-destructive testing (ndt): A review. Advances in Materials and Processing Technologies pp. 1–22 (2021)

[21] Harris, C.R., Millman, K.J., van der Walt, S.J., Gommers, R., Virtanen, P., Cournapeau, D., Wieser, E., Taylor, J., Berg, S., Smith, N.J., Kern, R., Picus, M., Hoyer, S., van Kerkwijk, M.H., Brett, M., Haldane, A., del Río, J.F., Wiebe, M., Peterson, P., Gérard-Marchant, P., Sheppard, K., Reddy, T., Weckesser, W., Abbasi, H., Gohlke, C., Oliphant, T.E.: Array programming with NumPy. Nature **585**(7825), 357–362 (Sep 2020). https://doi.org/10.1038/s41586-020-2649-2, `https://doi.org/10.1038/s41586-020-2649-2`

[22] He, Y., Li, Z., Fu, J., Wu, J., Ng, C.: Enhancing the performance of stochastic subspace identification method via energy-oriented categorization of modal components. Engineering Structures **233**, 111917 (2021)

[23] Hosseini, S.M., Mousa, S., Mohamed, H.M., Eslami, A., Benmokrane, B.: Experimental and analytical study on precast high-strength concrete tunnel lining segments reinforced with gfrp bars. Journal of Composites for Construction **26**(5), 04022062 (2022)

[24] Jeong, J.H., Jo, H., Laflamme, S., Li, J., Downey, A., Bennett, C., Collins, W., Taher, S.A., Liu, H., Jung, H.J.: Automatic control of ac bridge-based capacitive strain sensor interface for wireless structural health monitoring. Measurement **202**, 111789 (2022)

[25] Jiang, Y., Zhang, X., Taniguchi, T.: Quantitative condition inspection and assessment of tunnel lining. Automation in Construction **102**, 258–269 (2019). https://doi.org/https://doi.org/10.1016/j.autcon.2019.03.001

[26] Júnior, A., Lage, G.E., Caruso, N.C., Antonine, E., Lyra, P.H.: Development of a remote and low-cost bridge monitoring system. In: International Conference on Wave Mechanics and Vibrations. pp. 117–124. Springer (2023)

[27] Kandris, D., Nakas, C., Vomvas, D., Koulouras, G.: Applications of wireless sensor networks: an up-to-date survey. Applied System Innovation **3**(1), 14 (2020)

[28] Kapoor, N.R., Kumar, A., Arora, H.C., Kumar, A.: Structural health monitoring of existing building structures for creating green smart cities using deep learning. In: Recurrent Neural Networks, pp. 203–232. CRC Press

[29] Khazaee, M., Derian, P., Mouraud, A.: A comprehensive study on structural health monitoring (shm) of wind turbine blades by instrumenting tower using machine learning methods. Renewable Energy **199**, 1568–1579 (2022)

[30] Kullaa, J.: Detection, identification, and quantification of sensor fault in a sensor network. Mechanical Systems and Signal Processing **40**, 208–221 (2013)

[31] Kvåle, K.A., Øiseth, O., Rønnquist, A.: Operational modal analysis of an end-supported pontoon bridge. Engineering Structures **148**, 410–423 (2017)

[32] Lacidogna, G., Manuello, A., Carpinteri, A., Niccolini, G., Agosto, A., Durin, G.: Acoustic and electromagnetic emissions in rocks under compression. In: Experimental Mechanics on Emerging Energy Systems and Materials, Volume 5, pp. 57–64. Springer (2011)

[33] Lacidogna, G., Niccolini, G., Accornero, F., Carpinteri, A.: Acoustic emission wireless monitoring of structures. In: Acoustic emission and related non-destructive evaluation techniques in the fracture mechanics of concrete, pp. 19–48. Elsevier (2021)

[34] Lacidogna, G., Manuello, A., Niccolini, G., Carpinteri, A.: Acoustic emission monitoring of italian historical buildings and the case study of the athena temple in syracuse. Architectural Science Review **58**(4), 290–299 (2015)

[35] Liu, Z., Li, S., Guo, A., Li, H.: Comprehensive functional resilience assessment methodology for bridge networks using data-driven fragility models. Soil Dynamics and Earthquake Engineering **159**, 107326 (2022)

[36] López-Higuera, J.M., Cobo, L.R., Incera, A.Q., Cobo, A.: Fiber optic sensors in structural health monitoring. Journal of Lightwave Technology **29**, 587–608 (2011)

[37] Lu, F., Wang, H., Wang, L., Zhao, K., Zhang, J.: Degradation law and service life prediction model of tunnel lining concrete suffered combined effects of sulfate attack and drying–wetting cycles. Materials **15**(13), 4435 (2022)

[38] Manuello, A., Niccolini, G., Carpinteri, A.: Ae monitoring of a concrete arch road tunnel: Damage evolution and localization. Engineering Fracture Mechanics **210**, 279–287 (2019)

[39] Manuello Bertetto, A., Masera, D., Carpinteri, A.: Acoustic emission monitoring of the turin cathedral bell tower: Foreshock and aftershock discrimination. Applied Sciences **10**(11), 3931 (2020)

[40] Marano, G.C., Rosso, M.M., Aloisio, A., Cirrincione, G.: Generative adversarial networks review in earthquake-related engineering fields. Bulletin of Earthquake Engineering pp. 1–52 (2023)

[41] Melchiorre, J., Manuello, A., Marmo, F., Adriaenssens, S., Marano, G.: Differential formulation and numerical solution for elastic arches with variable curvature and tapered cross-sections. European Journal of Mechanics-A/Solids **97**, 104757 (2023)

[42] Melchiorre, J., Manuello, A., Sardone, L., Marano, G.C.: Damaging configurations in arch structures with variable curvature and tapered cross-section. WCCM-APCOM 2022 **900** (2022)

[43] Mishra, M., Lourenço, P.B., Ramana, G.V.: Structural health monitoring of civil engineering structures by using the internet of things: A review. Journal of Building Engineering **48**, 103954 (2022)

[44] Nagamani Devi, G., Vijayalakshmi, M.: Smart structural health monitoring in civil engineering: A survey. Materials Today: Proceedings **45**, 7143–7146 (2021), international Conference on Mechanical, Electronics and Computer Engineering 2020: Materials Science

[45] https://community.sw.siemens.com/s/article/OMG-What-is OMA-Operating-Modal-Analysis: "operational modal analysis"

[46] Pasca, D.P., Aloisio, A., Rosso, M.M., Sotiropoulos, S.: Pyoma and pyoma_gui: A python module and software for operational modal analysis. SoftwareX **20**, 101216 (2022). https://doi.org/https://doi.org/10.1016/j.softx.2022.101216

[47] Poulimenos, A., Fassois, S.: Parametric time-domain methods for non-stationary random vibration modelling and analysis — a critical survey and comparison. Mechanical Systems and Signal Processing **20**(4), 763–816 (2006). https://doi.org/https://doi.org/10.1016/j.ymssp.2005.10.003, `https://www.sciencedirect.com/science/article/pii/S0888327005001688`

[48] Rahaman, A., Park, C.H., Kim, B.: Design and characterization of a mems piezoelectric acoustic sensor with the enhanced signal-to-noise ratio. Sensors and Actuators A: Physical **311**, 112087 (2020)

[49] Rainieri, C., Fabbrocino, G.: Operational modal analysis of civil engineering structures. Springer, New York **142**, 143 (2014). https://doi.org/https://doi.org/10.1007/978-1-4939-0767-0

[50] Rao, A.R.M., Kasireddy, V., Gopalakrishnan, N., Lakshmi, K.: Sensor fault detection in structural health monitoring using null subspace–based approach. Journal of Intelligent Material Systems and Structures **26**(2), 172–185 (2015)

[51] Raschka, S.: Python Machine Learning. Packt Publishing - ebooks Account (2015), `http://www.amazon.com/exec/obidos/redirect?tag=citeulike07-20&path=ASIN/1783555130`

[52] Reis, M.S., Saraiva, P.M., Bakshi, B.R.: Data quality and denoising: A review (2020)

[53] Ren, H., Chen, X., Chen, Y.: Reliability based aircraft maintenance optimization and applications. Academic Press (2017)

[54] Rosso, M.M., Aloisio, A.: "classification performance of multi-layer perceptron network for damage-detection using subspace-based metrics"

[55] Rosso, M.M., Aloisio, A., Cucuzza, R., Pasca, D.P., Cirrincione, G., Marano, G.C.: Structural health monitoring with artificial neural network and subspace-based damage indicators. In: Trends on Construction in the Digital Era: Proceedings of ISIC 2022, pp. 524–537. Springer (2022)

[56] Rosso, M.M., Marasco, G., Aiello, S., Aloisio, A., Chiaia, B., Marano, G.C.: Convolutional networks and transformers for intelligent road tunnel investigations. Computers & Structures **275**, 106918 (2023)

[57] Rytter, A.: Vibrational Based Inspection of Civil Engineering Structures, vol. Fracture & dynamics Vol. R9314 No. 44. Aalborg University, Dept. of Building Technology and Structural Engineering (1993), ph.D. thesis

[58] Saeed, K., Mechbal, N., Coffignal, G., Vergé, M.: Subspace-based damage localization using artificial neural network. In: 18th Mediterranean Conference on Control and Automation, MED'10. pp. 563–568. IEEE (2010)

[59] Sarlo, R., Tarazaga, P.A., Kasarda, M.E.: High resolution operational modal analysis on a five-story smart building under wind and human induced excitation. Engineering Structures **176**, 279–292 (2018). https://doi.org/https://doi.org/10.1016/j.engstruct.2018.08.060, `https://www.sciencedirect.com/science/article/pii/S0141029617339007`

[60] Sun, M., Staszewski, W.J., Swamy, R.N.: Smart sensing technologies for structural health monitoring of civil engineering structures. Advances in Civil Engineering **2010**, 1–13 (2010)

[61] Taheri, S.: A review on five key sensors for monitoring of concrete structures. Construction and Building Materials **204**, 492–509 (2019)

[62] Tan, X., Chen, W., Zou, T., Yang, J., Du, B.: Real-time prediction of mechanical behaviors of underwater shield tunnel structure using machine learning method based on structural health monitoring data. Journal of Rock Mechanics and Geotechnical Engineering (2022)

[63] Thakur, A., et al.: A review on non-destructive techniques for corrosion monitoring in reinforced concrete structures. Recent Advances in Structural Engineering and Construction Management pp. 951–968 (2023)

[64] Tran, T.T., Ozer, E.: Synergistic bridge modal analysis using frequency domain decomposition, observer kalman filter identification, stochastic subspace identification, system realization using information matrix, and autoregressive exogenous model. Mechanical Systems and Signal Processing **160**, 107818 (2021)

[65] Wang, Q., Quek, S., Liew, K.: On the repair of a cracked beam with a piezoelectric patch. Smart Materials and Structures **11**(3), 404–410 (Jun 2002)

[66] Wang, Y.W., Ni, Y.Q., Wang, S.M.: Structural health monitoring of railway bridges using innovative sensing technologies and machine learning algorithms: a concise review. Intelligent Transportation Infrastructure (2022)

[67] Yan, A.M., Golinval, J.C.: Null subspace-based damage detection of structures using vibration measurements. Mechanical Systems and Signal Processing **20**(3), 611–626 (2006)

[68] Yu, Y., Wang, C., Gu, X., Li, J.: A novel deep learning-based method for damage identification of smart building structures. Structural Health Monitoring **18**, 143 – 163 (2018)

[69] Zhang, W., Qiu, J., Zhao, C.: Structural behavior degradation of corroded metro tunnel lining segment. Structure and Infrastructure Engineering pp. 1–17 (2022)

[70] Zhang, Y., Wang, M., Yu, L., Guo, X., Wang, Z., Li, C.: Experimental and numerical research on the influence of steel arch frame corrosion on security of supporting system in subsea tunnel. Tunnelling and Underground Space Technology **120**, 104253 (2022)

[71] Zhou, L., Sun, G., Li, Y., Li, W., Su, Z.: Point cloud denoising review: from classical to deep learning-based approaches. Graphical Models **121**, 101140 (2022)

[72] Zhou, X., Kim, C.W., Zhang, F.L., Chang, K.C.: Vibration-based bayesian model updating of an actual steel truss bridge subjected to incremental damage. Engineering Structures **260**, 114226 (2022)

[73] Zhu, L., Fu, Y., Chow, R., Spencer, B.F., Park, J., Mechitov, K.: Development of a high-sensitivity wireless accelerometer for structural health monitoring. Sensors (Basel, Switzerland) **18** (2018)

[74] Zhu, M., McKenna, F., Scott, M.H.: Openseespy: Python library for the opensees finite element framework. SoftwareX **7**, 6–11 (2018)